Does the regulation of local excitation-inhibition balance aid in recovery of functional connectivity? A computational account

Anirudh Vattikonda[1], S. Bapi Raju[1, 2], Arpan Banerjee[3], Gustavo Deco[4, 5], Dipanjan Roy[1]

[1]Cognitive Science Lab, International Institute of Information Technology, Hyderabad, India

[2]Center for Neural and Cognitive Sciences, University of Hyderabad, India

[3]Cognitive Brain Lab, National Brain Research Centre, NH8, Manesar, India

[4]Center for Brain and Cognition, Computational Neuroscience Group,

Department of Information and Communication Technologies, Universitat Pompeu Fabra, Roc Boronat 138, Barcelona, 08018, Spain

[5]Institució Catalana de Recerca i Estudis Avançats (ICREA), Universitat Pompeu Fabra, Passeig Lluís

Keywords: Resting state networks, Default mode, Virtual lesion, DMF model, Exc-Inh balance, functional connectivity

Abstract

Computational modeling of the spontaneous dynamics over the whole brain provides critical insight into the spatiotemporal organization of brain dynamics at multiple resolutions and their alteration to changes in brain structure (e.g. in diseased states, aging, across individuals). Recent experimental evidence further suggests that the adverse effect of lesions are visible on spontaneous dynamics characterized by changes in resting state functional connectivity and its graph theoretical properties (e.g. modularity). These changes originate from altered neural dynamics in individual brain areas that are otherwise poised towards a homeostatic equilibrium

to maintain a stable excitatory and inhibitory activity. In this work, we employ a homeostatic inhibitory mechanism, balancing excitation and inhibition in the local brain areas of the entire cortex under neurological impairments like lesions to understand global functional recovery (across brain networks and individuals). Previous computational and empirical studies have demonstrated that the resting state functional connectivity varies primarily due to the location and specific topological characteristics of the lesion. We show that local homeostatic balance provides a functional recovery by re-establishing excitation-inhibition balance in all areas that are affected by lesion. We systematically compare the extent of recovery in the primary hub areas (e.g. default mode network (DMN), medial temporal lobe, medial prefrontal cortex) as well as other sensory areas like primary motor area, supplementary motor area, fronto-parietal and temporo-parietal networks. Our findings suggest that stability and richness similar to the normal brain dynamics at rest is achievable by re-establishment of balance.

1. Introduction

Whole brain resting state dynamics at macroscopic scale provides a powerful approach to understanding key determinants of normal versus abnormal brain functions. Abnormal resting state brain dynamics characterized by changes in resting state functional connectivity (rs-FC) are observed in neurological disorders like epilepsy (Centeno and Carmichael, 2014; Holmes et al., 2013), Alzheimer's disease (Damoiseaux, 2012), Stroke (Park et al., 2011, Gratton et al., 2012), Schizophrenia (Yang et al., 2014) etc. Several theoretical models have been developed to understand the underlying mechanisms that allow such rich spontaneous dynamics to emerge (Deco et al., 2009, 2014, Hellyer et al., 2016). Local excitation and inhibition (E-I) balance or homeostasis is shown to play a key role in maintaining such rich dynamics. In this study we

47 investigate how local E-I balance is affected by structural perturbations and whether the same
48 mechanism can aid in functional recovery to normal rs-FC after a focal lesion is introduced in
49 the underlying structure. Previous work in this direction has sought out for computational tools
50 and graph theoretical techniques to investigate the precise impact on rs-FC under virtual lesions
51 in specific brain areas (both interhemispheric and intrahemispheric) (Alstottet al. (2009); Cabral
52 et al. (2012); Arsiwala et al. (2015)). Alstott et al. (2009) and subsequently, Cabral et al. (2012)
53 have independently investigated using computational models the nature of impact on rs-FC due
54 to perturbation in the structural connectivity (SC) similar to what is observed in brain lesions.
55 Further, Cabral et al. (2012) theoretical results suggest that most disconnection-related
56 neuropathology should induce the same qualitative changes in resting-state brain activity and
57 hence, finding common functional network alteration in the resting dynamics under a variety of
58 clinical conditions. These studies are the first ones to highlight the importance of lesion foci; for
59 example, hubs have a potentially damaging impact on the rs-FC to the point of a minimal
60 chance of recovery after lesion (Alstott et al., 2009; Arsiwalla et al., 2015). However, none of
61 the above studies account for fundamental processes like local homeostatic regulation of
62 inhibition providing right E-I balance to adapt to a target excitatory firing rate as a mechanism
63 for functional recovery. For the first time, we demonstrate systematically how this inhibitory
64 homeostasis aid in recovery across lesion foci (whether hub or not) using a variety of cortical
65 parcellations. Recently, Vogels et al., (2011) and Hellyer et al. (2016) have demonstrated in a
66 computational setup that inhibitory synaptic plasticity (a type of homeostatic plasticity) may
67 appropriately balance the excitatory and inhibitory currents of a cortical neuron, thereby
68 rendering it to produce a stable cortical output rather than runaway excitation. In Deco et al.
69 (2014), a feedback inhibition control (FIC) algorithm was proposed to adjust the strength of
70 inhibitory weights recursively and adapt to a target excitatory firing rate of 3 – 4 Hz. In this

study, we investigate how such local E-I balance is disturbed across multiple brain areas including hubs. What is the exact relationship between structural graph properties and the disturbed E-I balance? How widespread is the disturbed E-I balance depending on the lesion foci? We find that restoring the local E-I balance by using recursive adaptation of inhibitory weights in individual brain areas brings the local excitability to a stable firing range without compromising the richness of resting state dynamics and, as a result, reduces the damaging impact on rs-FC over the whole brain. Moreover, resting state networks are implicated in core process of human cognition like integration of cognitive and emotional processing (Greicius et al., 2003), monitoring the world around us (Gusnard et al., 2001) and mind-wandering (Mason et al., 2007). Hence we hypothesize that restoring rs-FC close to normality should aid in recovery from lesion.

2 Materials and Methods

2.1 Empirical Structural Connectivity

The empirical SC matrix used in this paper is generated by using an automated pipeline (Schirner et al., 2015) for reconstruction of fiber tracks from T1 structural MR images and diffusion-weighted images (DWI) acquired from 49 healthy subjects (30 females, 19 males) at Berlin Center for Advanced Imaging, Charité University Medicine, Berlin, Germany. The subjects' age ranged from 18 to 80 years with a mean age of 41.55 ± 18.44. The images obtained from these scans are used as input to the reconstruction pipeline to generate the SC matrix for each subject (Please refer to Schirner et al. (2015) for a detailed outline of the pipeline for generating SC matrix). In this pipeline, high resolution T1 anatomical images are used to create segmentation and parcellation of cortical and subcortical gray matter, white

matter segments and diffusion weighted imaging (DWI) for generating tractography masks. The major pre-processing steps on T1 anatomical images are skull stripping, removal of non-brain tissue, brain mask generation, cortical reconstruction, motion correction, intensity normalization, WM and subcortical segmentation, cortical tessellation generating GM–WM and GM-pia interface surface-triangulations and probabilistic atlas-based cortical and subcortical parcellation. These parcellations, segmentations and masks are then used to guide the probabilistic tractography algorithm to estimate connection strengths (a value in the range 0 to 1) between each pair of areas in the cortical gray matter parcellation. The parcellation used in this study is Desikan-Killiany parcellation (Desikan et al., 2006) which consists of 68 cortical regions of interest (ROI). SC matrices generated from each subject's MRI data are averaged element-wise to obtain an averaged SC matrix. The connectivity strength between each pair of 68 areas represents how one area can influence other areas in the context of a specific model (refer to section 2.4). To make sure results reported are robust to resolution of the parcellation and size of lesioned nodes, a SC matrix of 998 ROIs of approximately uniform size (Hagmann et al., 2008) generated from diffusion spectrum imaging of 5 healthy subjects is also used.

2.2 Empirical Resting State Functional Connectivity

Empirical rs-FC matrix is also generated using the same pipeline from the fMRI scans of the 49 subjects used for generating SC. The major steps involved in generating rs-FC matrix are brain extraction, motion correction, six-degrees of freedom (DOF) linear registration to the MNI space and high pass temporal filtering. The BOLD volumes are registered with subject's T1 weighted anatomical images and parcellated according to Desikan-Killiany atlas (Desikan et al., 2006). BOLD signals from each of the 68 ROIs are computed by taking the mean of BOLD signals of all voxels in that area. Aggregated BOLD time-series of each region is z-transformed and pairwise Pearson correlation coefficient is computed to obtain the rs-FC matrix of each

subject. The FC matrix used in this study is the average of rs-FC matrices of all 49 subjects. Also since we only use resting state functional data in this study, we use the words functional connectivity (FC) and resting state functional connectivity (rs-FC) synonymously.

2.3 Simulating virtual focal Lesions

Focal lesions damage the anatomical structural connectivity of the brain in a specific area or in and around a specific area. In order to simulate a focal lesion in area *i* (lesion center), all the connections to and from that area are set to zero in the SC matrix, i.e., all the entries in row *i* and column *i* of SC matrix are set to zero. An example of virtually lesioned SC matrix with left Precuneus as the lesion center is shown in **Fig. 1.** To understand the characteristics of lesion location that critically impact rs-FC, 68 virtually lesioned SC matrices are generated with focal virtual lesions at each one of the 68 ROIs. For the SC matrix of 998 ROIs a focal lesion in area *i* is simulated by disconnecting (set to zero) all connections to and from 50 nearest neighbours (5% of total) in addition to connections of lesion center. Lesions centered at 40 different locations (20 in each hemisphere) covering 80 – 90 % of the cerebral cortex are simulated resulting in 40 lesioned SC matrices at a resolution of 998 ROIs. These matrices are then downsampled to 66 areas by averaging across ROIs (For details on downsampling refer to Hagmann et al., 2008 , Honey et al., 2008).

2.4 Computational Model simulating whole brain resting state dynamics

Mean field models (Wilson and Cowan, 1972, Wong and Wang, 2006, Deco et al., 2009, Hellyer et al, 2016) allow simulation of whole brain dynamics and are analytically tractable unlike models for networks of spiking neurons. Using mean filed models earlier research have shown that rs-FC can be estimated from the SC matrix using a large scale cortical dynamic mean field (DMF) model (Deco et al., 2014) and a hemodynamic model (Friston et al., 2000; Friston et al., 2003). The DMF model is a set of coupled stochastic differential equations which

govern the evolution of synaptic gating variables with time (Deco et al., 2014). The hemodynamic model is a set of coupled differential equations which can predict the BOLD responses of a neural population given the synaptic activity of that population. Using the generated BOLD responses from each area, FC can be estimated by computing Pearson correlation coefficient between BOLD responses of each pair of areas. The pipeline used to compute FC using anatomical SC matrix and computational modeling is shown in **Fig. 2**.

Dynamic Mean Field Model: In DMF model, each brain area is modeled as a population of excitatory and inhibitory neurons with excitatory NMDA synapses and inhibitory GABA synapses. The computational model for simulating the synaptic activity is given by the set of coupled stochastic nonlinear differential equations given below (Deco et al., 2014).

$$I_i^{(E)} = W_E I_0 + w_+ J_{NMDA} + G J_{NMDA} \sum_j C_{ij} S_j^{(E)} - J_i S_i^{(I)} \quad (1)$$

$$I_i^{(I)} = W_I I_0 + J_{NMDA} S_i^{(E)} - S_i^{(I)} \quad (2)$$

$$r_i^{(E)} = \frac{a_E I_i^{(E)} - b_E}{1 - \mathrm{e}^{(-d_E (a_E I_i^{(E)} - b_E))}} \quad (3)$$

$$r_i^{(I)} = \frac{a_I I_i^{(I)} - b_I}{1 - \mathrm{e}^{(-d_I (a_I I_i^{(I)} - b_I))}} \quad (4)$$

$$\frac{dS_i^{(E)}}{dt}(t) = -\frac{S_i^{(E)}}{\tau_E} + (1 - S_i^{(E)}) \gamma r_i^{(E)} + \sigma v_i(t) \quad (5)$$

$$\frac{dS_i^{(I)}}{dt}(t) = -\frac{S_i^{(I)}}{\tau_I} + r_i^{(I)} + \sigma v_i(t) \quad (6)$$

Here $I_i^{(E \text{ or } I)}$, is the input current to area i and superscripts E and I represent excitatory and inhibitory populations in that area. $r_i^{E \text{ or } I}$ is the population firing rate of excitatory or inhibitory populations of area i, $S_i^{E \text{ or } I}$ is the average synaptic gating variable of area i. I_0 is the effective external input scaled by W_E and W_I for excitatory and inhibitory populations. J_{NMDA} is the

excitatory synaptic coupling and J_i is the local feedback inhibitory synaptic coupling. v_i in Eq. 5,6 is uncorrelated standard Gaussian noise with noise amplitude σ = 0.001 nA. The input currents to an excitatory population in an area are: recurrent excitatory currents, recurrent inhibitory currents, long range excitatory currents from excitatory populations in all other areas, and external currents. Long range excitatory currents from other areas to an excitatory population in area *i* are constrained by the connectivity strength from those areas given by C_{ij}, where C_{ij} is the ij^{th} entry in the SC matrix. Since recurrent excitatory currents are already taken into account while computing the input current to an excitatory population all the diagonal elements, C_{ii}, are set to zero in the SC matrix. The connectivity strengths C_{ij} are scaled by a global coupling parameter *G*. A parameter sweep for various values of *G* is performed to compute the optimal value of *G* for which the simulated FC-estimate best correlates with that computed from the empirical resting-state fMRI data of healthy controls. The input currents to an inhibitory population in area *i* are: recurrent excitatory currents, recurrent inhibitory currents, external currents. All the parameters of the model are set to same values as in Deco et al. (2014) and summarized in **Table 2**. Furthermore, in order to maintain a steady state firing rate of 2 – 5 Hz, the input current to excitatory population is maintained such that $I_i^E - b_E/a_E = -0.026$ nA(see Eq. 3) by the Feedback Inhibition Control (FIC) algorithm, as proposed in Deco et al. (2014). The FIC algorithm iteratively adjusts J_i values representing synaptic coupling from inhibitory neurons to excitatory neurons, to maintain the input current at an excitatory population equal to $b_E/a_E - 0.026$ nA, with a tolerance of ± 0.005 nA. Hence we consider local excitation-inhibition balance to be established in an area when the input current to an excitatory pool is in the above range. By numerically solving the differential equations in this model using Euler's method with a step size of 0.1 ms for 8 minutes we generated the synaptic activity of each area and used

this activity as input to the hemodynamic model (Friston et al., 2000, Friston et al., 2003) to generate the resting-state BOLD responses of each brain area. Although we used a time step of 0.1 milliseconds in Euler's method, we sampled the synaptic activity from each area every 1 millisecond. First 500 ms of BOLD responses are truncated to allow for initial transients and the rest is downsampled every 2 s to get a resolution similar to empirical BOLD time series. All simulations are performed using MATLAB.

DMF model parameter space identification and calibration

Global coupling strength G is a free parameter of DMF model that scales long range excitatory input. In order to estimate the optimal value of G that best predicts resting dynamics, DMF model is simulated with increasing values of G starting from 0 and at increments of 0.025. The model generated FC is compared against empirical FC by calculating the fit between them as Pearson correlation coefficient between the z-transformed upper diagonal elements. The correlation fit between simulated FC and empirical FC as a function of the free parameter G is shown in **Fig. 3A**. The optimal value of G is that which gives best correlation fit between empirical and simulated FC while maintaining the firing rate in the range of 3 - 5 Hz in all brain regions. For the SC of 68 areas best correlation fit of 0.6 between simulated and empirical FC while maintaining a low firing rate is observed when $G = 0.6$. The firing rate of all regions at this optimal value of G is shown in **Fig. 3B.** As can be seen in this figure, a low firing rate of about 4 Hz is maintained in all areas in the balanced excitation-inhibition condition. Empirical FC and model-generated FC obtained by simulating DMF model with G set to 0.6 are shown in **Fig. 3C and D** respectively. G is set to 0.6 in all the simulations performed in further analysis throughout the entire paper unless otherwise specified. For values of $G > 0.6$ firing rate of many areas exceed 20 Hz and hence the model is not bio-physically realistic.

2.5 Measures for characterizing lesioned nodes and for effects of lesion on FC

To characterize areas into hubs or connector nodes, graph theoretical measures, namely, *participation coefficient* and *node strength* are used. Brain Connectivity Toolbox (Rubinov and Sporns, 2010) is used to compute both these measures. Frobenius norm of the difference between model predicted FC matrix and empirical FC matrix is used to measure the dynamic effects of a lesion on FC

Participation Coefficient: Given the modular organization of a graph *participation coefficient* of each node in that graph can be computed (Guimera and Amaral, 2005). Participation coefficient measures how well distributed the links of a node are to other modules. If the links of a node are uniformly distributed to all modules then its participation coefficient is 1, whereas if all its links are within its own module then participation coefficient is 0. So nodes with participation coefficient close to 1 are considered as connector nodes. Eq. 7 describes how to compute the participation coefficient of i^{th} node, where N_M is the number of modules, k_{is} is the number of links of node i to module s and k_i is the total number of links of node i.

$$P_i = 1 - \sum_{s=1}^{N_M} \left(\frac{k_{is}}{k_i} \right) \tag{7}$$

Node Strength is the sum of connection strengths of all connections to that area. Nodes with high node strength are shown to have relatively large effect on FC when lesioned compared with nodes with low node strength (Alstott et al., 2009). Eq. 8 describes how to compute node strength of i^{th} area, where N is the number of ROIs.

$$Strength(area_i) = \sum_{j=1}^{N} C_{ij} \tag{8}$$

Note that for higher resolution SC, participation coefficient and node strength are computed as summation of participation coefficient and node strength respectively of all 50 disconnected ROIs for each lesion.

FC Distance (FCD): In order to measure the similarity or distance between the model predicted FC and the empirical FC, we have used the Frobenius norm of the difference between the two FC matrices.

$$FCD = \sqrt{\sum_{i=1}^{N}\sum_{j=1}^{N} \left| FCEmpirical(i,j) - FCModel(i,j) \right|^2} \quad (9)$$

Higher the FC Distance, higher the damaging impact of lesion on FC. Similarly, lower the FC Distance, lower is the impact. Eq. 9 describes how FC distance between these two matrices is computed.

Z-score: We used Z-scores to test the hypothesis that whether the functional correlations of any pair of ROI before and after lesion are from different distributions. Before computing the Z-scores we have converted both FC matrices, predicted by DMF model using healthy controls SC and lesioned SC, to normal distribution by using Fisher's z-transform. Z-score between functional correlation of area *i* and *j* is computed as

$$Z_{ij} = \frac{(r_{ij}^{healthy} - r_{ij}^{lesioned})}{\sqrt{\left(\frac{1}{df-3} + \frac{1}{df-3}\right)}} \quad (10)$$

Where, *df* is the effective degrees of freedom and it is equal to 230 (length of simulated BOLD time series) for all the simulations in this study. To find a threshold for Z-score above which correlations are considered to have come from different distributions, we have computed Z-

scores between correlations of two FC matrices generated by averaging FC from two sets of 5 independent runs of model using healthy controls SC. For $|Z| > 2$ the error rate is zero, hence Z-scores ($|Z|$) greater than 2 are considered to have significantly changed.

2.6 Measuring immediate effects of lesion on FC

We define *immediate effects* as those effects on FC that are caused by a lesion, before processes like plasticity set in to recover the damage caused by lesion. We are not directly modeling plasticity but rather the E-I balance that maintains local homeostasis. In fact, E-I balance has been shown to be related to inhibitory synaptic plasticity (Vogels et al., 2011). Hence, we consider the effects due to a lesion in SC matrix on the FC before re-establishing E-I balance as immediate effects. We start with an E-I balanced network of healthy subjects and study the effect of acute brain injury or lesion on these networks. In order to measure the immediate effects on FC arising from a lesion in one of the 68 ROIs, we have used the following procedure (refer to the model described by Eq. 1-6): 1) We have computed the J_i values, i.e., local feedback inhibitory synaptic coupling, of each brain area by running the DMF model with FIC algorithm using the averaged SC of healthy controls. These are the values that maintain E-I balance before lesion. 2) Using these J_i values and a virtually lesioned SC in DMF model we generated the FC as described above in the model section. 3) Finally, we compute FC Distance between empirical FC and model generated FC to quantify the effects of a particular lesion on FC. Note that step 1 is a one-time process, as the SC of healthy controls does not change, however steps 2 and 3 must be run for each lesioned SC.

2.7 Re-establishing Excitation-Inhibition balance after a lesion

In this study we show that the impact of cortical lesions on functional connectivity can be reduced by re-establishing E-I balance. Recall that E-I balance would be perturbed by such lesions. After virtually lesioning an ROI we observe that many other ROIs lose E-I balance

causing immediate effect on FC. We hypothesize that if E-I balance is re-established after lesion then the impact of lesion on FC would be reduced. In order to investigate this we use the following procedure: 1) We have initialized the J_i values i.e., local feedback synaptic coupling weights with the values obtained by running DMF model with FIC on the averaged SC of healthy controls. 2) Using the lesioned SC we run the DMF model with FIC to re-establish E-I balance in all the areas. 3) To measure the similarity between model-generated FC and empirical FC, we compute the FC distance between these two matrices. Again step 1 is a one-time process whereas steps 2 and 3 are repeated for each virtually lesioned SC matrix.

3 RESULTS

3.1 Effects of lesion on E-I balance

An area, say *i*, is considered to have E-I balance if $I_i^E - \frac{b_E}{a_E} = -0.026$ nA with a tolerance of ±0.005 nA(see Materials and Methods), where I_i^E is excitatory input current to area *i*, b_E and a_E are intrinsic parameters used in estimating average firing rate of an excitatory population (Deco et al., 2014). Hence we consider an area to have lost E-I balance if $|I_i^E - \frac{b_E}{a_E} + 0.026| > 0.005$, where $|x|$ is the absolute value of *x*. **Fig. 4A** shows that local E-I balance is perturbed in many areas when SC, obtained with left Precuneus (lPCUN) as the lesion center, is used in the DMF model. **Fig. 4B** shows the number of areas that have lost E-I balance for each of the 68 brain areas as lesion centers in the virtually lesioned SC matrix. We then investigated the relationship between lesioned area's participation coefficient and the effect on E-I balance. **Fig. 4C** exhibits, lesions in areas with high participation coefficient perturb

balance in a wider number of areas. Participation Coefficient and number of areas that have lost E-I balance have shown a strong correlation of 0.61 ($p < 0.001$) (see **Fig. 4C**). To make sure that the results observed are not due to non-uniform lesion sizes, correlation between participation coefficient and number of areas that lost E-I balance is investigated on a SC of higher resolution with 40 lesions of uniform size (see Materials and Methods). Similar results are observed (**Fig. S1 A**) with a correlation of 0.56 ($p < 0.001$)

3.2 Immediate effects of lesion on functional connectivity

Next we investigated the immediate effects on FC for each lesion center. In order to predict the immediate effects on FC we have initialized the inhibitory synaptic weights (J_i) with the values corresponding to E-I balanced condition. Then a specific focal lesion is incorporated in the SC matrix and the resulting FC is generated using the DMF model (see Materials & Methods). We then computed the FC distance between the model-predicted FC and empirical FC. The FC distance is found to be strongly correlated to the participation coefficient and node strength of the lesion center. Node strength and FC Distance showed a correlation of 0.87 ($p < 0.001$) and participation coefficient and FC Distance showed a correlation of 0.62 ($p < 0.001$) (see **Fig. 6A and B (black)**). Same relationship is observed even when the lesions are of uniform size (**Fig. S1 B**). This finding is consistent with previous studies (Alstott et al., 2009) i.e., if the lesioned area is a hub or connector node (that has high participation coefficient or node strength) then the effects due to a lesion on FC are generally large. Although in the main text we highlight the recovery process based on lesion center in lPCUN, several experiments with lesion centers in other areas were conducted and the results are similar (See Supplementary Material and Table 3)

3.3 Functional recovery after re-establishing E-I balance

After re-establishing local E-I balance in all areas, by simulating the DMF model with FIC and initializing J_i with those generated by simulating DMF model with FIC on SC of healthy controls (see Materials & Methods), we found that the impact of lesion on FC is significantly reduced compared to the immediate impact of lesion (shown in previous section) on FC. For example, FC predicted by the DMF model using a virtually lesioned SC with lesion center as lPCUN before and after re-establishing E-I balance are shown in **Fig. 5**. The FC predicted by model after re-establishing E-I balance is similar to the empirical FC than the FC predicted by the model before re-establishing E-I balance. Unlike in the case of immediate impact of lesion on FC, we found that by re-establishing E-I balance in all areas FC Distance is not so strongly correlated with participation coefficient and node strength of lesioned area. This is illustrated by reduced correlations between node strength, participation coefficient and FC Distance to 0.25 (p = 0.04) and 0.03 (p = 0.82), respectively as shown in **Fig. 6A, B (blue)**. The results are again validated using a SC with lesions of uniform size (**Fig. S1 B**). Previous studies (Alstott et al., 2009) have shown that lesion impact is higher when the lesioned area is near cortical midline. We found that even when areas near the cortical midline (PCUN, CAC) are lesioned, by re-establishing E-I balance the effects of lesion on FC have been largely reduced. Table 3 gives a summary of effects of lesions in cortical midline, parietal and temporal cortex, frontal cortex, sensory, motor cortex. **Fig. 7 (top)** shows the functional connections that have significantly changed ($|z| > 2$) immediately after a lesion in cortical midline (lCAC). By re-establishing E-I balance the number of connections that have significantly changed have been largely reduced as shown in **Fig. 7 (bottom)**. One important observation to be noted is that the impact of lesion on intra-hemispheric connections is reduced drastically after re-establishing E-I balance. Similar results are observed for lesions in frontal cortex (CMF) and parietal cortex (IP) as shown in supplementary material (see **Fig. S2, S3**). It can be clearly seen that the number of connections

that have significantly changed are drastically reduced after re-establishing E-I balance. This shows that compared to the FC predicted by DMF model immediately after lesion, there is a significant FC recovery after E-I balance is re-established.

FC Recovery across subjects:

FC recovery across subjects is compared by using SC of 5 different subjects. First, optimal value of G is computed for each subject's SC. Optimal value of G varied across subjects in the range 0.5 to 0.8. For all 5 subjects, FC recovery results are qualitatively similar to the average SC case i.e. even when hubs are lesioned, after re-establishing E-I balance the effects of lesion on FC are largely reduced. **Fig. 8** shows how FC distance varies across subjects before and after re-establishing E-I balance when regions which are more likely to be hubs (participation coefficient > 0.5) are lesioned. Finally, we looked at how local inhibitory weights of each area (J_i values) changed across lesion location after re-establishment of E-I balance. To investigate this relationship, correlation between updated J_i value of an area for each lesion and particpation coefficient of the lesion center is computed. For all areas, the updated J_i values showed strong correlation ($r > 0.35$, $p < 0.001$) with participation coefficient of lesioned location. Hence we posit that when hubs are lesioned there is an increased excitatory activity in all areas driving the dynamics towards a high excitatory regime.

4 Discussion

Whole brain computational modeling is becoming increasingly popular for gaining a deeper neurophysiological understanding of complex brain functions. In particular, assessing the effect of short-range (recurrent connectivity) and long-range (inter/intra-hemispheric) input during

resting and task conditions may provide valuable insight into resources allocated to processing noisy as well as structured information (Deco, G. et al., 2014; Deco, G. & Kringelbach, M. L et al., 2014; Roy et al., 2014). The brain regulates such information flow from region to region based on principles of integration as well as segregation (Deco et al., 2015). We argue that whole-brain computational modeling based on underlying anatomical connectivity obtained from neuroimaging data can be used to gain new insights into such segregation and integration processes. The motivation for our present study stems from the need for understanding whether recurrent inhibitory weight up-and-down regulation meaning homeostasis can indeed aid in functional recovery to normalcy under a variety cortical lesions spread over multiple lesion centers. However there are several limitation to this study. Firstly unlike recently implemented by Hellyer et al. (2016) inhibitory plasticity is not directly modeled however all the ingredients are present and the underlying homeostatic mechanisms are qualitatively very similar to qualify this as a good candidate for inhibitory plasticity. While their whole purpose of introducing inhibitory plasticity is to predict accurately empirical FC our's is not. We are carefully looking at the departure from E-I balanced regime due to change in excitation resulted from a lesion. This may vary across subjects and lesion centers. Hence, we make a comparison between how the recurrent inhibitory weights change based on location of lesion foci and across participants. We do find variability in the adaptation time to the appropriate J_i values based on the size or location of the lesion but not significant variability across participants. For the overall mathematical tractability which was established in our earlier work with this model (Deco et al. (2014); Roy et al. (2014)) DMF model is chosen in the current work.

One of the major advantages of using DMF model is that it allows for tracking mathematically long-range excitatory inputs to relevant brain areas either due to variation in the global coupling strength or by the perturbation introduced by the lesioned SC. In a recent study (Yang et al.,

2014), such a large-scale mathematical model has been used to show key model parameters global coupling strength, recurrent self-excitatory weights might be responsible for the empirically observed high power of the total signal in schizophrenia patients. In this work, we regulate the recurrent inhibitory weights in individual brain areas for the maintenance of regional E-I balance under focal lesion. We quantify the lesion impact on E-I balance area wise using the correlation between participation coefficient of lesioned area and the degree of perturbation in the E-I balance. Our investigation is carried out over the entire Cerebral Cortex much like in the spirit of previous lesion modeling attempts made by Alstott et al. (2009); Cabral et al. (2012), Arshiwala et al. (2015), Adhikari et al. (2015). For the first time, our study systematically characterizes departure from healthy E-I balance (**Fig. 4 A,B,C**) due to focal lesions in brain modules (hub areas like DMN, FPN and sensory areas like Visual, Motor, etc.). Further, it is computationally demonstrated how cortical recovery to normalcy is possible using a simple local inhibitory homeostasis mechanism (similar to inhibitory plasticity as proposed by Helleyer et al. (2016)) with lesion centers covering over 80% of the cerebral cortex (**Table 2**). We have shown that upon lesioning a node which acts as a hub or connector node there is a widespread disruption in the regional E-I balance (see **Table 1**; rPCUN, rPC, rISTH, rCAC, lPCUN, lPC, lISTH, lCAC prefixes r,l stand for right and left hemisphere respectively). Interestingly, these areas are located in the vicinity of Supplementary motor area (SMA), Primary motor cortex (M1) which are directly affected following focal lesions in stroke patients. We have shown that immediate effects of an injury on FC are significant when the lesioned node is a hub using a similarity measure such as FC distance (see Material and Methods). This finding is consistent with the previous computational studies (Alstott et al., 2009; Arsiwalla et al., 2015). We have also shown that upon re-establishing E-I balance in all areas excluding lesioned area the effects of an injury on FC are dramatically reduced even when

414 the lesioned area is a hub. We believe this finding is of importance in designing strategies for
415 brain network recovery. Virtual lesions generated in this study are focal (composed of default
416 mode brain areas, frontoparietal, temporoparietal junctions) that are commonly found in
417 structural aberrations present in the stroke (Awad et al., 1986). Previously lesions of posterior
418 medial cortex (PMC) were described as rare, but resulting in profound disorders of
419 consciousness (Damasio et al., (1999)), while lesions of the dorsal anterior cingulate cortex
420 (dACC) resulted in severe disruptions of personality and even emotional processing, resulting in
421 apathy and inattention (Bush et al., (2000)). Lesions in the vicinity of temporoparietal junctions
422 have been found to be affecting language-related disorders, in particular, the left angular gyrus
423 has been implicated in dyslexia (Horwitz et al. (2002)), while lesions centered on the posterior
424 position of right superior temporal cortex (rSTC) often result in spatial hemineglect (Karnath et
425 al., (2001)). Our modeling approach in the present article indeed demonstrates computationally
426 to recover from the widespread spatial disruption induced by lesioned brain areas. Moreover,
427 our model suggests that the pattern of endogenous neural activity, in particular, the default
428 mode network activity (DMN) can be restored to a significant extent (see **Table 2**). DMN has
429 been implicated as a common brain network involved in the pathophysiology of aging and
430 neurodegenerative disorders such as schizophrenia, Alzheimers, autism spectrum disorders
431 (Douaud, G. et al., (2014)). An eventual restoration of the topology of resting-state FC may aid
432 in cognitive repair and recovery.
433 One more limiting fact of our study is that, although, we have theortically shown that recovery
434 is possible by re-establishing E-I balance, the biological time scale of such process is an open
435 question. Biologically how long would it take (meaning time scale) for recurrent inhibitory
436 weights to adapt to a value such that input to the excitatory pool equal to $I_i^E - b_E / a_E = -0.026$

nA i.e., slightly inhibitory dominated, leading to a target firing rate equal to 3.0631 Hz is difficult to answer? We have checked the variability of J_i values as a function of the lesion center and subject wise to get an idea of the numerical time scale of adaptation. Finally, it is also important to consider the differences in the recovery processes across lesion locations as well as the difference in simulated FC following re-establishment of E-I balance and healthy control FC. E-I balance plays a key role in maintaining stable neuronal activity and proper cortical function. Dynamic interaction between excitatory and inhibitory inputs was shown to maintain neural networks in a balanced state that favors neural computations (McCormick, 2002; Haider and McCormick, 2009). We have shown that stable neuronal activity after a lesion is attained by re-establishing E-I balance, through appropriate regulation of the strength of local inhibition in individual brain areas. However, even after re-establishing E-I balance the FC is not completely similar to healthy controls FC, as evident from **Fig. 7**, **Fig. S2** and **Fig. S3**, suggesting that there might be some irrecoverable components, which may result in subtle differences in a given task performance. Also, the degree of FC recovery as measured by FCD in **Fig. 8A, B** is not exactly uniform across lesion locations implying that different lesions may still cause different subtle behavioural deficits based on lesion location. Apart from maintaining E-I balance, inhibition in local cortical circuits is also shown to play a key role in gain modulation (Mitchell and Silver, 2003), improving the dynamic range of input representation (Liu et al., 2011) in cortex, tuning of cortical neurons to sensory stimuli (Wilent and Contreras, 2005; Wang et al., 2000) and pacing oscillations that allow propagation of neuronal signals (Atallah and Scanziani, 2009; Hasenstaub et al., 2005). Hence changes in the strength of local inhibition, while maintaining E-I balance, may have an effect on information representation and transmission in cortex and discrimination performance of the incoming stimuli. One way to quantify the differences after recovery that potentially impacts information transmission

efficacy and stimulus discrimination ability is to measure multi-scale entropy, mutual information or Fisher information. Further, network measures based on graph theory such as local efficiency, global efficiency may provide valuable insights into how information routing changes after reestablishing E-I balance. Existing studies using empirical neuroimaging data from stroke patients have already shown that there is a change in the modular organization of resting state functional networks post-stroke (Gratton et al., 2012). Hence a systematic investigation of graph theoretic properties of FC after re-establishing balance might be a fruitful avenue for a future study. Another intriguing possibility is to look at the fitting of optimal underlying structural connectivity (SC) based on recovered functional connectivity (FC) using an optimization algorithm proposed in Deco et al. (2014b). Compared to normal FC re-established FC may be working at a different working point of the global workspace. In this study the long-range coupling strength (G) is kept fixed at 0.6 for all simulations; however, post-stroke SC determines how the global coupling value G is shifted in the parameter space. In Deco et al. (2014b), a dramatic improvement of the fitting of the matrices was obtained with the addition of a small number of anatomical links, particularly cross-hemispheric connections, and reweighting of existing connections. Like previous study, we suggest that the notion of a critical working point 'G', where the structure-function interplay is maximal, may provide a new way to link behaviour and cognition, and a new perspective to understand recovery of function under variety of clinical conditions.

Currently, longitudinal data acquisition from stroke patients is underway, and it may be possible to find out how long it would take for meaningful biological recovery. As a future application we would like to integrate our study into the Virtual Brain Neuroinformatics Platform (Leon et al., 2013; Ritter et al., 2013; Roy et al., 2014) and would be made available to the clinicians. Recovery from a variety of lesion locations may allow clinicians to introduce virtual surgery

and simulate the resulting brain dynamics before actually taking any relevant decisions. To match the real-time clinical settings the size of the simulation will have to be significantly scaled, and complexity of the model needs to take into account more brain regions, different neurotransmitters, inhibitory subtypes. Here, the replicability of our finding is checked with multiple levels of granularity of the connectivity data (coarser to finest resolution). If methods to directly measure the target excitation value in a population are available, it might be possible to use techniques such as Transcranial Magnetic Stimulation (TMS), Transcranial Direct Current Stimulation (tDCS) to look at the variability of the excitatory population firing rate with the size and location of the inhibited brain hot spots. In conclusion, in this paper we provide a direct functional benefit of inhibitory homeostatic regulation to bring back the functional connectivity to normalcy and provide stability without compromising the richness and complexity of spatiotemporal dynamics in the brain.

Acknowledgements

This study was funded by A.B. Ramalingaswami fellowship (BT/RLF/Re-entry/31/2011) and Innovative Young Bio-technologist Award (IYBA), (BT/07/IYBA/2013) from Department of Biotechnology, Ministry of Science & Technology, Government of India. GD is supported by the ERC Advanced Grant: DYSTRUCTURE (n. 295129), by the Spanish Research Project PSI2013-42091-P. and funding from the European Union Seventh Framework Programme (FP7-ICT Human Brain Project (grant no. 60402)).

References

Adhikari, M. H., Beharelle, A. R., Griffa, A., Hagmann, P., Solodkin, A., McIntosh, A. R., ... & Deco, G. (2015). Computational Modeling of Resting-State Activity Demonstrates Markers of

Normalcy in Children with Prenatal or Perinatal Stroke. *The Journal of Neuroscience*, *35*(23), 8914-8924.

Alstott, J., Breakspear, M., Hagmann, P., Cammoun, L., & Sporns, O. (2009). Modeling the impact of lesions in the human brain. *PLoS Comput Biol*, *5*(6), e1000408-e1000408.

Arsiwalla, X. D., Zucca, R., Betella, A., Martinez, E., Dalmazzo, D., Omedas, P., ... & Verschure, P. F. (2015). Network dynamics with BrainX3: a large-scale simulation of the human brain network with real-time interaction. *Frontiers in neuroinformatics*, *9*.

Awad, I., Modic, M., Little, J. R., Furlan, A. J., & Weinstein, M. (1986). Focal parenchymal lesions in transient ischemic attacks: correlation of computed tomography and magnetic resonance imaging. *Stroke*,*17*(3), 399-403.

Bush, G., Luu, P., & Posner, M. I. (2000). Cognitive and emotional influences in anterior cingulate cortex. *Trends in cognitive sciences*, *4*(6), 215-222.

Cabral, J., Hugues, E., Kringelbach, M. L., & Deco, G. (2012). Modeling the outcome of structural disconnection on resting-state functional connectivity.*Neuroimage*, *62*(3), 1342-1353.

Centeno, M., & Carmichael, D. W. (2014). Network connectivity in epilepsy: resting state fMRI and EEG–fMRI contributions. *Frontiers in neurology*, *5*.

Damoiseaux, J. S. (2012). Resting-state fMRI as a biomarker for Alzheimer's disease. *Alzheimers Res Ther*, *4*(8).

Damasio, A., & Dolan, R. J. (1999). The feeling of what happens. *Nature*,*401*(6756), 847-847.

Deco, G., Jirsa, V., McIntosh, A. R., Sporns, O., & Kötter, R. (2009). Key role of coupling, delay, and noise in resting brain fluctuations. *Proceedings of the National Academy of Sciences*, *106*(25), 10302-10307.

Deco, G., & Jirsa, V. K. (2012). Ongoing cortical activity at rest: criticality, multistability, and ghost attractors. *The Journal of Neuroscience*, *32*(10), 3366-3375.

Deco, G., Ponce-Alvarez, A., Mantini, D., Romani, G. L., Hagmann, P., & Corbetta, M. (2013). Resting-state functional connectivity emerges from structurally and dynamically shaped slow linear fluctuations. *The Journal of Neuroscience*, *33*(27), 11239-11252.

Deco, G., Ponce-Alvarez, A., Hagmann, P., Romani, G. L., Mantini, D., & Corbetta, M. (2014). How Local Excitation–Inhibition Ratio Impacts the Whole Brain Dynamics. *The Journal of Neuroscience*, *34*(23), 7886-7898.

Deco, G., McIntosh, A. R., Shen, K., Hutchison, R. M., Menon, R. S., Everling, S., ... & Jirsa, V. K. (2014). Identification of optimal structural connectivity using functional connectivity and neural modeling. *The Journal of Neuroscience*, *34*(23), 7910-7916.

Deco, G., & Kringelbach, M. L. (2014). Great expectations: using whole-brain computational connectomics for understanding neuropsychiatric disorders.*Neuron*, *84*(5), 892-905.

Deco, G., Tononi, G., Boly, M., & Kringelbach, M. L. (2015). Rethinking segregation and integration: contributions of whole-brain modelling. *Nature Reviews Neuroscience*, *16*(7), 430-439.

Desikan, R. S., Ségonne, F., Fischl, B., Quinn, B. T., Dickerson, B. C., Blacker, D., ... & Killiany, R. J. (2006). An automated labeling system for subdividing the human cerebral cortex on MRI scans into gyral based regions of interest.*Neuroimage*, *31*(3), 968-980.

Douaud, G., Groves, A. R., Tamnes, C. K., Westlye, L. T., Duff, E. P., Engvig, A., ... & Johansen-Berg, H. (2014). A common brain network links development, aging, and vulnerability to disease. *Proceedings of the National Academy of Sciences*, *111*(49), 17648-17653.

Friston, K. J., Harrison, L., & Penny, W. (2003). Dynamic causal modelling.*Neuroimage*, *19*(4), 1273-1302.

Friston, K. J., Mechelli, A., Turner, R., & Price, C. J. (2000). Nonlinear responses in fMRI: the Balloon model, Volterra kernels, and other hemodynamics. *NeuroImage*, *12*(4), 466-477.

Gratton, C., Nomura, E. M., Pérez, F., & D'Esposito, M. (2012). Focal brain lesions to critical locations cause widespread disruption of the modular organization of the brain. *Journal of cognitive neuroscience*, *24*(6), 1275-1285.

Guimera, R., & Amaral, L. A. N. (2005). Functional cartography of complex metabolic networks. *Nature*, *433*(7028), 895-900.

Hagmann, P., Cammoun, L., Gigandet, X., Meuli, R., Honey, C. J., Wedeen, V. J., & Sporns, O. (2008). Mapping the structural core of human cerebral cortex. *PLoS Biol*, *6*(7), e159.

Hellyer, P. J., Jachs, B., Clopath, C., & Leech, R. (2016). Local inhibitory plasticity tunes macroscopic brain dynamics and allows the emergence of functional brain networks. *NeuroImage*, *124*, 85-95.

Holmes, M. J., Yang, X., Landman, B. A., Ding, Z., Kang, H., Abou-Khalil, B., ... & Morgan, V. L. (2013). Functional networks in temporal-lobe epilepsy: a voxel-wise study of resting-state functional connectivity and gray-matter concentration. *Brain connectivity*, *3*(1), 22-30.

Honey, C. J., Sporns, O., Cammoun, L., Gigandet, X., Thiran, J. P., Meuli, R., & Hagmann, P. (2009). Predicting human resting-state functional connectivity from structural connectivity. *Proceedings of the National Academy of Sciences*,*106*(6), 2035-2040.

Horwitz, B., Rumsey, J. M., & Donohue, B. C. (1998). Functional connectivity of the angular gyrus in normal reading and dyslexia. *Proceedings of the National Academy of Sciences*, *95*(15), 8939-8944.

Karnath, H. O., Ferber, S., & Himmelbach, M. (2001). Spatial awareness is a function of the temporal not the posterior parietal lobe. *Nature*, *411*(6840), 950-953.

606 Leon, P. S., Knock, S. A., Woodman, M. M., Domide, L., Mersmann, J., McIntosh, A. R., &
607 Jirsa, V. (2013). The Virtual Brain: a simulator of primate brain network dynamics. *Frontiers in*
608 *neuroinformatics*, *7*.
609
610 Liu, B. H., Li, Y. T., Ma, W. P., Pan, C. J., Zhang, L. I., & Tao, H. W. (2011). Broad inhibition
611 sharpens orientation selectivity by expanding input dynamic range in mouse simple cells.
612 *Neuron*, *71*(3), 542-554.
613
614 Mitchell, S. J., & Silver, R. A. (2003). Shunting inhibition modulates neuronal gain during
615 synaptic excitation. *Neuron*, *38*(3), 433-445.
616
617 Park, C. H., Chang, W. H., Ohn, S. H., Kim, S. T., Bang, O. Y., Pascual-Leone, A., & Kim, Y.
618 H. (2011). Longitudinal changes of resting-state functional connectivity during motor recovery
619 after stroke. *Stroke*, *42*(5), 1357-1362.
620
621 Ritter, P., Schirner, M., McIntosh, A. R., & Jirsa, V. K. (2013). The virtual brain integrates
622 computational modeling and multimodal neuroimaging. *Brain connectivity*, *3*(2), 121-145.
623
624 Roy, D., Sigala, R., Breakspear, M., McIntosh, A. R., Jirsa, V. K., Deco, G., & Ritter, P. (2014).
625 Using the virtual brain to reveal the role of oscillations and plasticity in shaping brain's
626 dynamical landscape. *Brain connectivity*, *4*(10), 791-811.
627
628 Rubinov, M., & Sporns, O. (2010). Complex network measures of brain connectivity: uses and
629 interpretations. *Neuroimage*, *52*(3), 1059-1069.
630

631 Schirner, M., Rothmeier, S., Jirsa, V. K., McIntosh, A. R., & Ritter, P. (2015). An automated
632 pipeline for constructing personalized virtual brains from multimodal neuroimaging data.
633 *NeuroImage*.
634
635 Schoonheim, M. M., Geurts, J. J., Landi, D., Douw, L., van der Meer, M. L., Vrenken, H., ... &
636 Stam, C. J. (2013). Functional connectivity changes in multiple sclerosis patients: a graph
637 analytical study of MEG resting state data.*Human brain mapping*, *34*(1), 52-61.
638
639 Vogels, T. P., Sprekeler, H., Zenke, F., Clopath, C., & Gerstner, W. (2011). Inhibitory plasticity
640 balances excitation and inhibition in sensory pathways and memory networks. *Science*,
641 *334*(6062), 1569-1573.
642
643 Wang, J., Caspary, D., & Salvi, R. J. (2000). GABA -A antagonist
644 of tuning in primary auditory cortex. *Neuroreport*, *11*(5), 1137-1140.
645
646 Wilent, W. B., & Contreras, D. (2005). Dynamics of excitation and inhibition underlying
647 stimulus selectivity in rat somatosensory cortex. *Nature neuroscience*, *8*(10), 1364-1370.
648
649 Wilson, H. R., & Cowan, J. D. (1972). Excitatory and inhibitory interactions in localized
650 populations of model neurons. *Biophysical journal*, *12*(1), 1.
651
652 Wong, K. F., & Wang, X. J. (2006). A recurrent network mechanism of time integration in
653 perceptual decisions. *The Journal of neuroscience*, *26*(4), 1314-1328.
654

Xia, M., Wang, J., & He, Y. (2013). BrainNet Viewer: a network visualization tool for human brain connectomics. *PloS one*, *8*(7), e68910.

Yang, G. J., Murray, J. D., Repovs, G., Cole, M. W., Savic, A., Glasser, M. F., ... & Anticevic, A. (2014). Altered global brain signal in schizophrenia.*Proceedings of the National Academy of Sciences*, *111*(20), 7438-7443.

Figures and Tables Captions:

Figure 1: Simulating focal lesions. In order to simulate lesion in an area all the connections to and from that area are set to zero. **A**, Averaged structural connectivity matrix of healthy subjects and the **B**, Lesioned structural connectivity with lesion center as left Precuneus(PCUN) **C**, All the 68 brain areas plotted as spheres according to their Talairach coordinates on the brain surface with all their connections, size of spheres represent the participation coefficient of that area with larger size representing larger participation coefficient. **D**, The connections in C that are removed or set to zero when lesioned area is left Precuneus are shown in red.

Figure 2: General Pipeline to elucidate estimation of functional connectivity from anatomical structural connectivity. Using the anatomical structural connectivity (SC) obtained from DTI scans, the Dynamic Mean Field (DMF) model generates the synaptic activity for each ROI. These activities are fed as input to Balloon-Windkessel hemodynamic model to generate BOLD time series for each area and finally pairwise Pearson correlation coefficient is calculated to obtain the resting state functional connectivity (FC).

Figure 3: Parameter space exploration for optimal value of global coupling strength (*G*) and network dynamics generated by simulating dynamic mean field model with feedback inhibition control using the averaged structural connectivity of 49 healthy subjects: **A**, Correlation fit between simulated functional connectivity and empirical functional connectivity for average SC of healthy controls for various values of global coupling strength. *G*=0.6 (green cross) produced the best correlation fit of 0.6 while maintaining a low firing rate in all areas. **B**, Firing rate of all regions is maintained below 5 Hz by recursively adjusting the local feedback inhibition weights. **C**, Averaged empirical functional connectivity of 49 healthy subjects. **D**, Model predicted resting state functional connectivity using optimal value of *G* and averaged SC of healthy controls.

Figure 4: Effects of lesion on E-I balance: Immediately after lesioning, many areas lost their local E-I balance. **A-left,** *E-I balance test condition** value for each of the 68 brain regions immediately after lesioning left Precuneus. **A-right,** *E-I balance test condition** values of each area after re-establishing E-I balance. The red line indicates the value below which E-I balance is maintained. **B**, Number of areas that lost local E-I balance with each of the 68 brain regions as lesion center. The number of areas that lost local E-I balance is strongly correlated with the participation coefficient of the lesion center. **C**, Correlation between participation coefficient of each lesion center and the number of areas that lost local E-I balance.

*E-I balance test condition** value for an area ***i*****:** $\left| I_i^E - \frac{b_E}{a_E} + 0.026 \right|$

Figure 5: Functional connectivity predicted by DMF model using a virtually lesioned structural connectivity matrix with lesion center as left Precuneus **A**, immediately after lesion i.e without re-establishing E-I balance. **B**, after re-establishing E-I balance

Figure 6: Immediate lesion effects and recovery of functional connectivity after cortical lesion. The immediate effects of lesion are strongly correlated with lesion measures: lesioned Node Strength and Participation Coefficient. **A** (black), **B** (black), Correlation between FC Distance and Lesioned Node Strength, FC Distance and Participation Coefficient. FC Distances are computed between model predicted functional connectivity immediately after lesioning each of the 68 brain regions and empirical functional connectivity. **A** (blue), **B** (blue), Correlation between FC Distance and Lesioned Node Strength, FC Distance and Participation Coefficient. FC Distances are computed between model predicted functional connectivity after re-establishing E-I balance in all areas and empirical functional connectivity.

Figure 7: Number of connections that significantly changed ($|Z| > 2$), see Materials and Methods, due to lesion in right CAC. The top 3 figures display connections that have significantly changed before re-establishing local E-I balance. The bottom 3 figures represent the connections that have significantly changed after re-establishing local E-I balance. In the lateral view of left and right hemispheres only intra-hemispheric connections are shown while in the dorsal view of the whole brain (middle panel) inter hemispheric connections are also shown. The effects of lesion on both hemispheres have been drastically reduced by re-establishing E-I balance. The number of connections that significantly changed within ipsi-lateral hemisphere is reduced by 97% and within contra-lateral hemisphere by 100%.

Figure 8: FC recovery to normalcy across subjects and lesion location. FC Distance across subjects is plotted for lesions at nodes with participation coefficient > 0.5. **A**, FC Distance across subjects and lesion location immediately after lesion. **B**, FC Distance across subjects and lesion location after re-establishing E-I balance.

Table 1: List of all 34 ROIs in each hemisphere. AreaID represents the order of ROIs in the structural and functional connectivity matrices for each hemisphere.

Table 2: DMF model parameters and their values used in simulations.

Table 3: FC Distance (FCD) before and after re-establishing local E-I balance with lesion centers in cortical midline, parietal and temporal cotrex, frontal cortex, sensory and motor cortex. For areas highlighted in bold (lIP, lCMF, rCAC. Here prefixes r, l stand for right and left hemisphere respectively) the functional connections that have significantly changed from healthy controls functional connections are shown in supplementary figures.

Figures and Tables:

Figure 1:

A

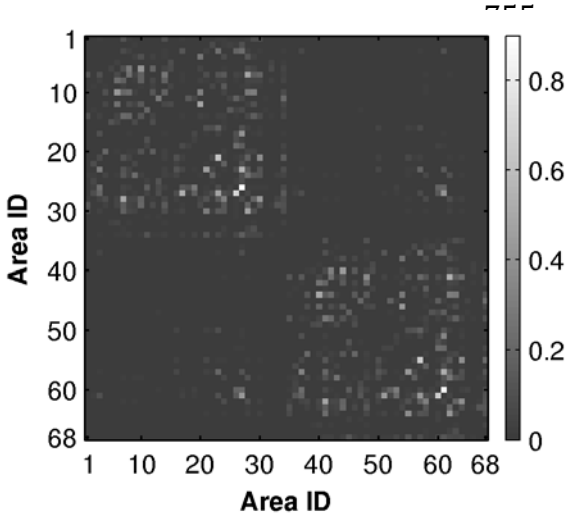

B

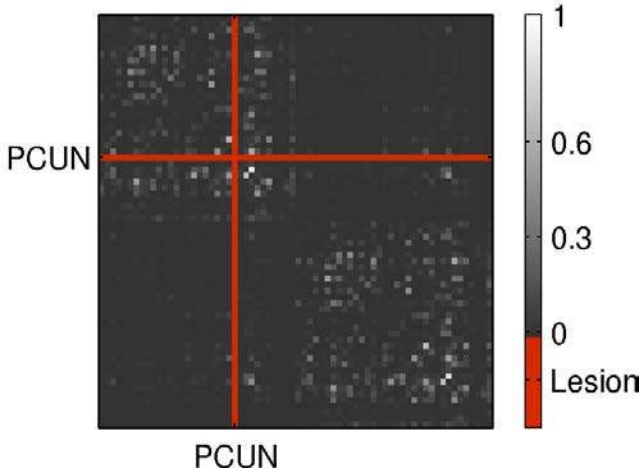

C

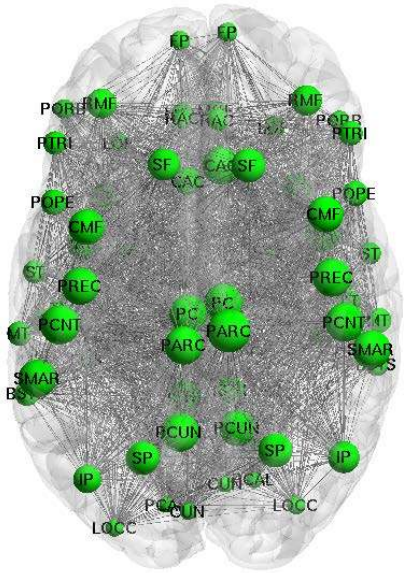

D

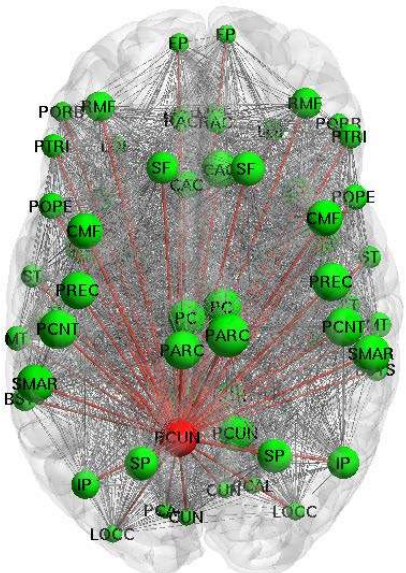

Figure 2:

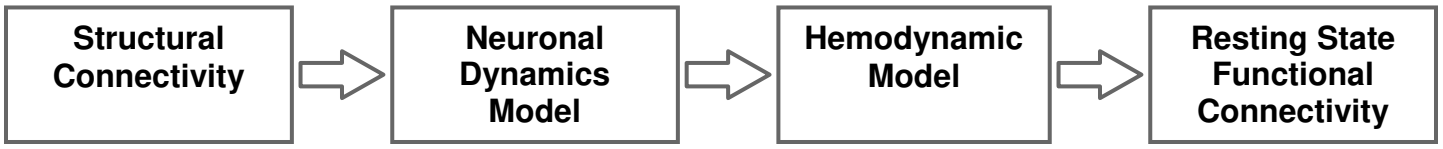

Figure 3:

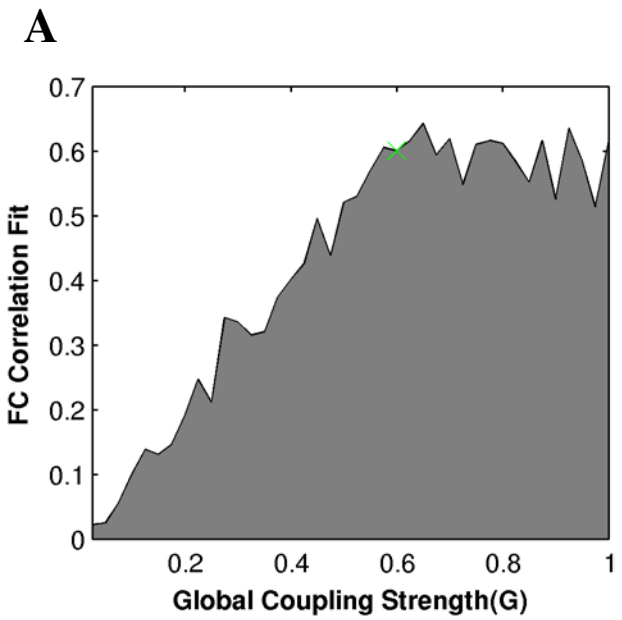

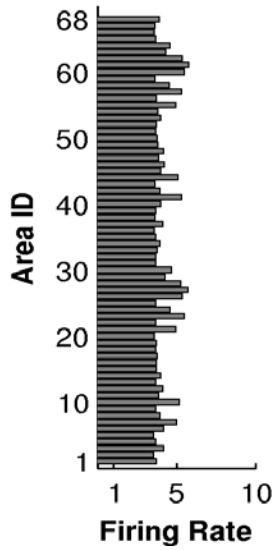

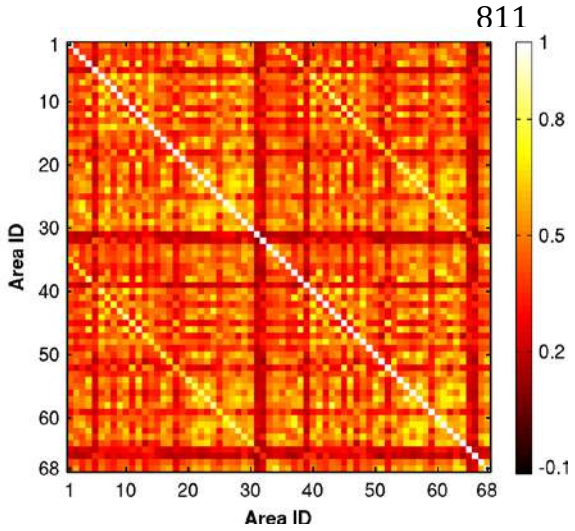

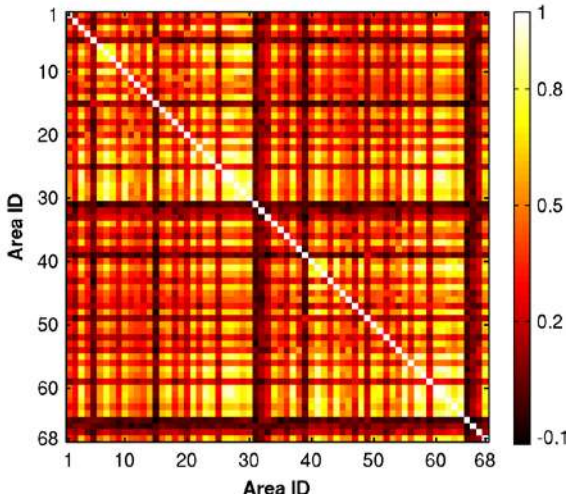

Figure 4:

A

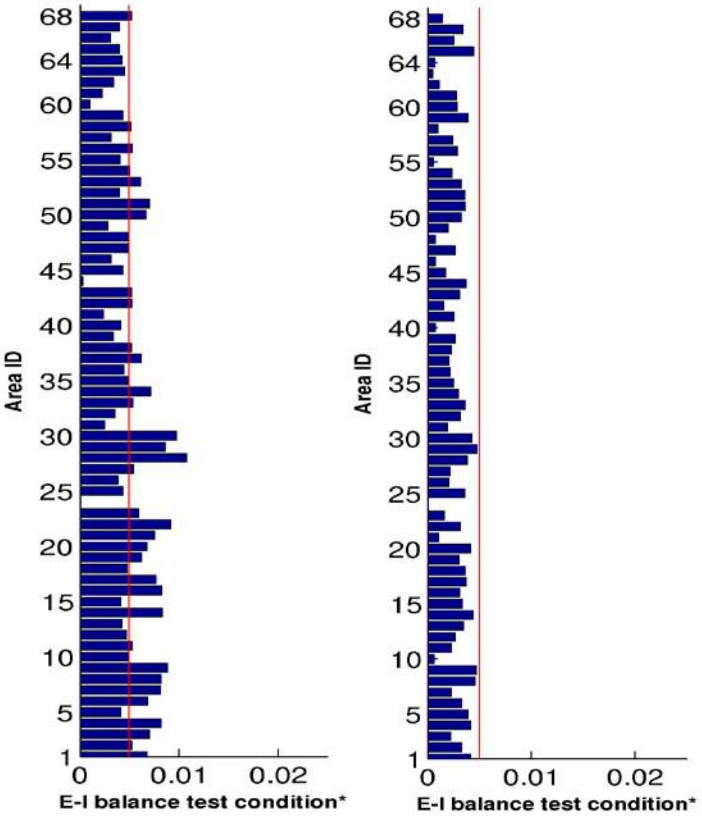
Area ID
E-I balance test condition*
Area ID
E-I balance test condition*

B

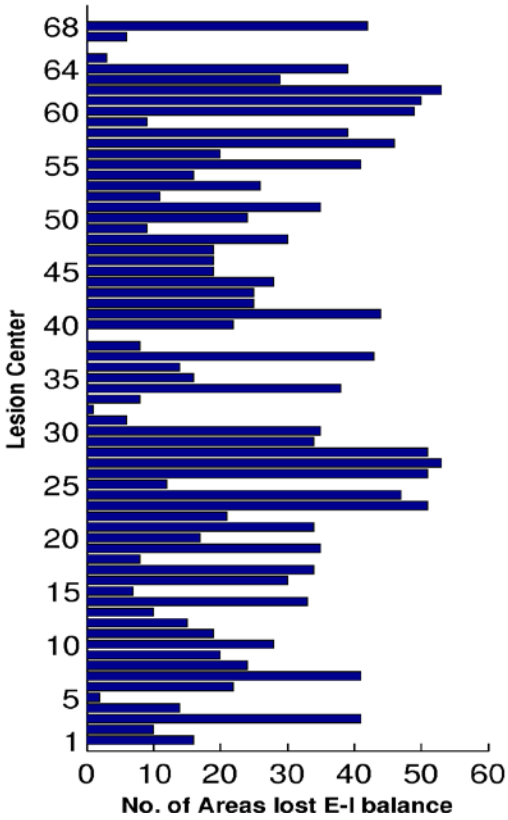
Lesion Center
No. of Areas lost E-I balance

C

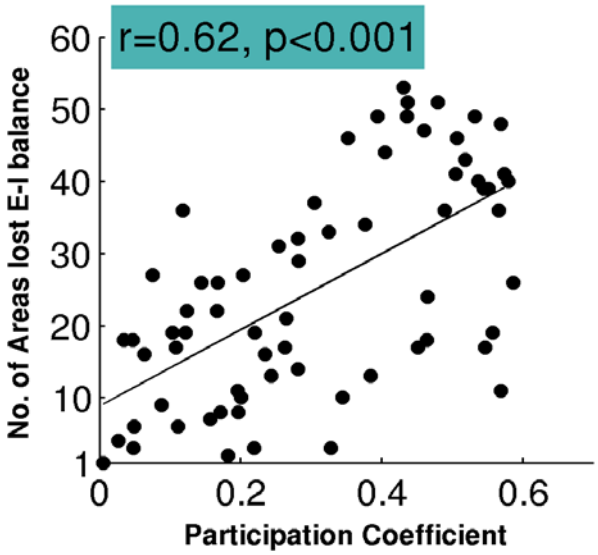
r=0.62, p<0.001
No. of Areas lost E-I balance
Participation Coefficient

Figure 5:

A **B**

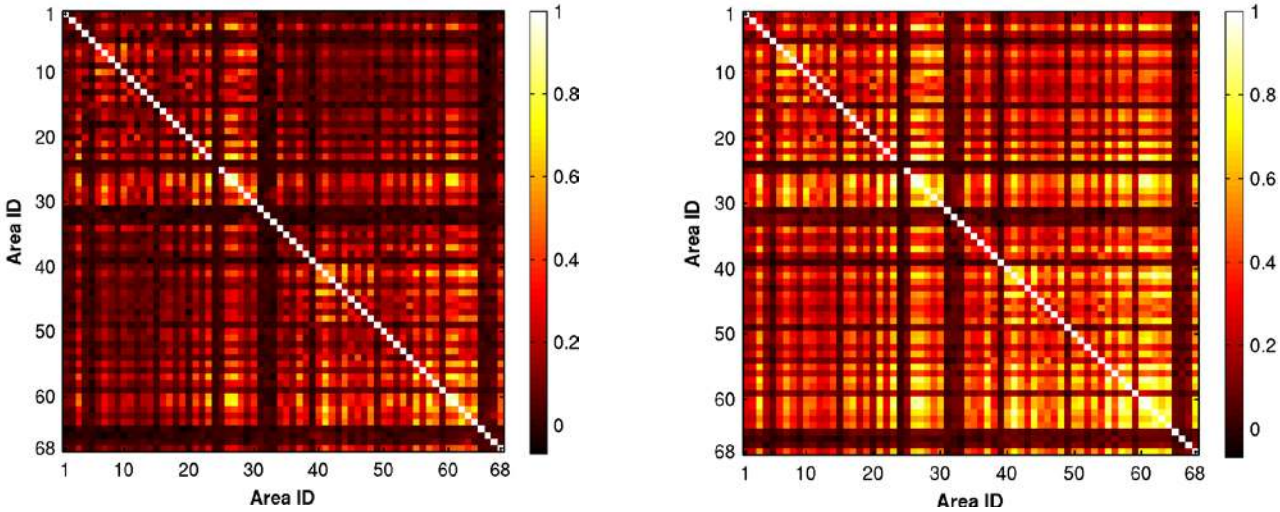

Figure 6:

A **B**

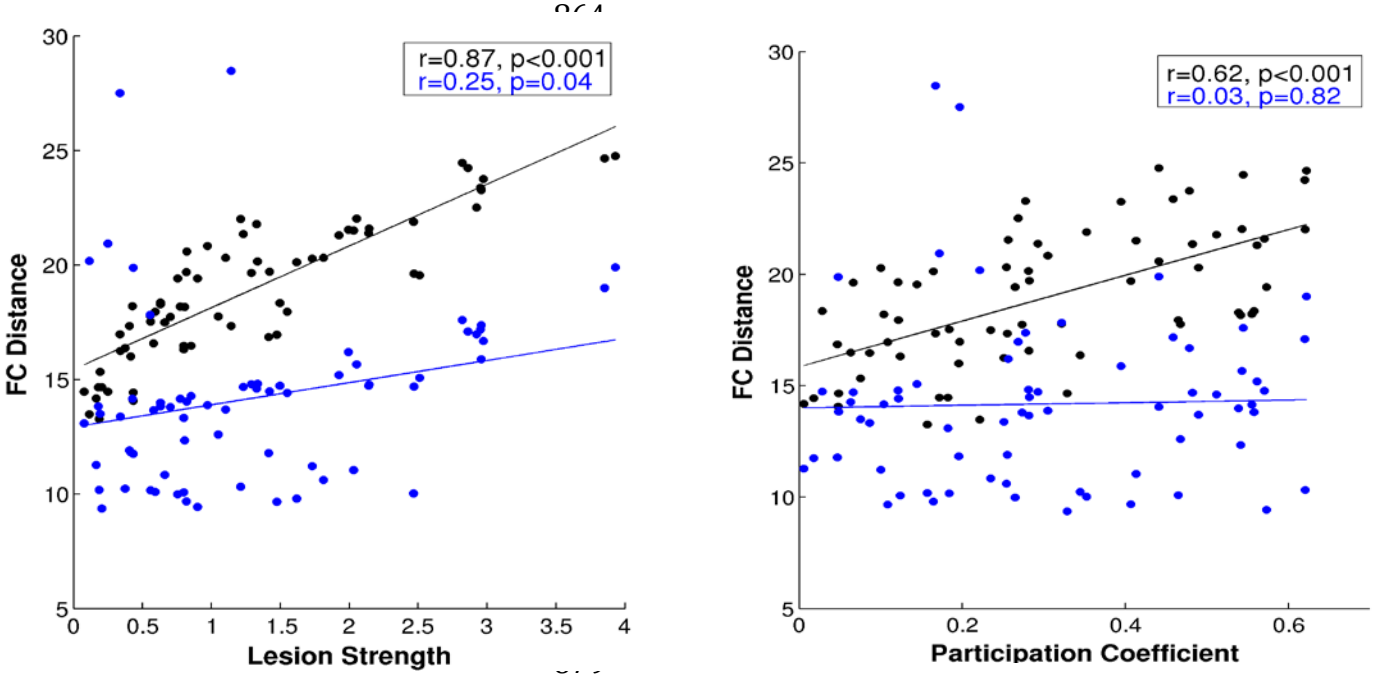

Figure 7:

Figure 8:

A

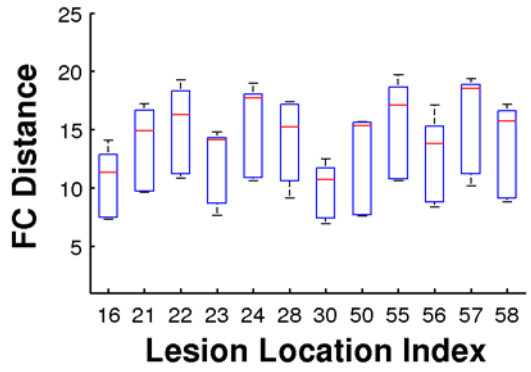

B

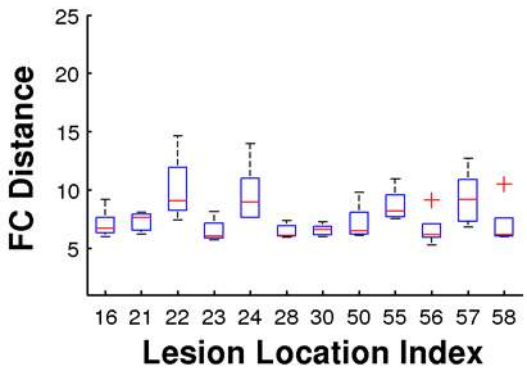

Table 1:

Area ID	Abbreviation	Full Name
1	BSTS	Banks Of Superior Temporal Sulcus
2	CAC	Caudal Anterior Cingulate
3	CMF	Caudal Middle Frontal
4	CUN	Cuneus
5	ENT	Entorhinal
6	FUS	Fusiform
7	IP	Inferior Parietal
8	IT	Inferior Temporal
9	ISTH	Isthmus Cingulate
10	LOCC	Lateral Occipital
11	LOF	Lateral Orbito Frontal
12	LING	Lingual
13	MOF	Medial Orbito Frontal
14	MT	Middle Temporal
15	PARH	Parahippocampal
16	PARC	Paracentral
17	POPE	Pars Opercularis
18	PORB	Pars Orbitalis
19	PTRI	Pars Triangularis
20	PCAL	Pericalcarine
21	PCNT	Post Central
22	PC	Posterior Cingulate
23	PREC	Precentral
24	PCUN	Precuneus
25	RAC	Rostral Anterior Cingulate
26	RMF	Rostral Middle Frontal
27	SF	Superior Frontal
28	SP	Superior Parietal
29	ST	Superior Temporal
30	SMAR	Supra Marginal
31	FP	Frontal Pole
32	TP	Temporal Pole
33	TT	Transverse Temporal
34	INS	Insula

Table 2:

DMF Model Parameters
Excitatory:
$W_E = 1,\ \ w_+ = 1.4,\ \ J_{NMDA} = 0.15$ nA
$a_E = 310$ nC^{-1}, $\ b_E = 125$ Hz, $\ d_E = 0.16$ s
Inhibitory:
$W_I = 0.7,\ \ a_I = 615$ nC^{-1}, $\ b_I = 177$ Hz
$d_I = 0.087$ s
Kinetic:
$\gamma = 0.641$ s, $\ \tau_E = 100$ ms, $\ \tau_I = 10$ ms

Table 3:

	Area	Participation Coefficient	FCD before re-establishing E-I balance	FCD after re-establishing E-I balance
Left Hemisphere				
Cortical midline	PCUN	0.57	21	15
	CAC	0.34	16	10
Parietal and Temporal cortex	**IP**	**0.35**	**22**	**10**
	SMAR	0.55	22	16
	ST	0.25	20	11
	IT	0.28	20	15
Frontal cortex	SF	0.43	25	20
	CMF	**0.51**	**22**	**15**
	POPE	0.3	21	14
Sensory, Motor	LOCC	0.14	20	15
	PREC	0.53	24	18
Right Hemisphere				
Cortical midline	PCUN	0.51	22	11
	CAC	**0.54**	**18**	**14**
Parietal and Temporal cortex	IP	0.43	23	17
	SMAR	0.55	22	16
	ST	0.23	20	11
	IT	0.25	20	15
Frontal cortex	SF	0.47	25	19
	CMF	0.51	22	10
	POPE	0.29	21	14
Sensory,Motor	LOCC	0.16	20	15
	PREC	0.56	24	17